Nuclear Medicine and Biomedical Imaging

Research Article

Advanced magnetic resonance imaging and the contribution of ^{99m}*Tc-tetrofosminbrain* SPECT in the differential diagnosis of cerebral tumors

Tsitsia V[1], Valotassiou V[2], Kapsalaki E[3], Fountas K[4], Siasios I[4], Tzavara C[2], Theodorou K[1], Georgoulias P[2] and Tsougos I[1]*

[1]Medical Physics Department, Faculty of Medicine, University of Thessaly, Biopolis, Larissa 41110, Greece

[2]Department of Nuclear Medicine, Faculty of Medicine, University of Thessaly, Biopolis, Larissa 41110, Greece

[3]Department of Radiology, Faculty of Medicine, University of Thessaly, Biopolis, Larissa 41110, Greece

[4]Department of Neurosurgery, Faculty of Medicine, University of Thessaly, Biopolis, Larissa 41110, Greece

Abstract

Objective: Differential diagnosis between brain lesions is essential for the patients' treatment approach but may be challenging based only on conventional diagnostic methods. The aim of our study was to evaluate the diagnostic effectiveness of the advanced MRI techniques proton magnetic resonance spectroscopy (^{1}HMRS), dynamic susceptibility contrast imaging (DSCI), diffusion-weighted imaging (DWI), diffusion tensor imaging (DTI) and the contribution of *^{99m}Tc-Tetrofosmin brain* single-photon emission computed tomography **(***SPECT***)** *in the differential diagnosis of cerebral tumors.*

Methods: Thirty six patients *underwent ^{1}H-MRS, DWI, DTI and DSCE MRI followed by ^{99m}Tc-Tetrofosmin brain SPECT within the same week. Early and delayed ^{99m}Tc-Tetrofosmin SPECT images were compared with the metabolites' ratios derived by ^{1}H-MRS,* apparent diffusion coefficient (ADC) *and fractional anisotropy* **(***FA***)** *derived by DWI and DTI respectively and relative* cerebral blood volume (*rCBV*) *derived by DSC MRI. The multi-parametric results were confirmed by the histopathological findings.*

Results: Both early and delayed *^{99m}Tc-Tetrofosmin SPECT indices significantly correlated with rCBV. Moreover,* delayed *^{99m}Tc-Tetrofosmin* SPECT lesion to normal (L/N) ratios were significantly increased compared to early SPECT L/N ratios in glioblastomas, while metastases and meningiomas presented stable or slightly decreasing tracer uptake. There were significant differences in N-acetylaspartate to creatine ratio (NAA/Cr), FA and ADC values among the diagnoses and a cut-off value of 0.11 for FA could discriminate low from high grade tumors.

Conclusion: Delayed *^{99m}Tc-Tetrofosmin* brain SPECT compared to early *^{99m}Tc-Tetrofosmin* brain SPECT images showed promise in the differential diagnosis between high and low grade tumors, especially when combined with advanced MR techniques.

Introduction

Neuroimaging has evolved from a purely anatomy-based specialty to a multi-parameter discipline that combines morphologic abnormalities with hemodynamic information, intra-cellular microstructure and cellular metabolism.

Advanced MR neuroimaging includes ^{1}HMR spectroscopy which is a powerful noninvasive imaging technique that provides important in vivo metabolic information, complementing morphological findings from conventional MRI in the clinical setting. Proton magnetic resonance spectroscopy has proved useful in grading low and high-grade gliomas as well in differentiating active tumor from therapy-related necrosis, but it should always be considered a supplementary tool to the patients' clinical history and conventional MRI when reaching the final diagnosis [1]. In addition to ^{1}H-MRS, perfusion imaging has already found increasing use in the evaluation of brain tumors as it allows some insight into angiogenesis, a process that is present in a number of hypoxic and ischemic conditions in the central nervous system and an important factor in malignant primary tumors. Neoplastic induced angiogenesis results in structurally abnormal vessels which in turn develop an increased macro- and microvasculature, in comparison to healthy brain tissue [2]. Neoplasms have increased permeability parameters on perfusion MR images and the increase of the rCBV is found to correlate with aggressive tumor growth, thus it facilitates the prediction of brain lesion progression in conjunction with histopathology [1,3]. Diffusion imaging and Diffusion Tensor imaging still remains a subject of intense research. Diffusion imaging has been shown to be an imaging biomarker for assessing tumor aggressiveness and early response to therapy in neoplasms as it probes local tissue microstructure and provides a sensitive means to detect alterations in the integrity of white matter structures [4,5]. Moreover DTI, the evolution of DWI, has the potential to give a complete picture of the neuronal architecture as water molecules diffuse differently along the tissues depending on its type, integrity and presence of barriers, giving information about its orientation and quantitative anisotropy [6].

Correspondence to: Ioannis Tsougos, Medical Physics Department, University Hospital of Larissa, Biopolis, 41110 Larissa, Greece, E-mail: tsougos@med.uth.gr

Key words: *^{99m}Tetrofosmin brain SPET, advanced MRI techniques, brain tumors, differential diagnosis*

Received: November 12, 2018; **Accepted:** November 23, 2018; **Published:** November 29, 2018

The incorporation of the aforementioned advanced MRI techniques that provide specific physiologic information on the morphology, the degree of vascularity and the Blood Brain Barrier (BBB) rupture as well as the microstructure and metabolic changes of the lesions, has given the opportunity to neuro-radiologists to combine meaningful biomarkers for the assessment of malignancy. However, MRI techniques alone still face several limitations on the assessment of cell proliferation and hence the characterization of intracranial tumors as well as the differentiation between residual/recurrent tumors and treatment-related changes.

Therefore, the introduction of Nuclear Medicine modalities which provide information on the proliferative activity and metabolic features of the brain lesions is of major importance in the clinical evaluation of intracranial lesions. Positron emission tomography is the state-of-the-art nuclear modality as it presents higher spatial resolution, compared to SPET, as well as increased accuracy and considerably enhancing sensitivity. Although SPET presents several drawbacks, such as low-resolution images prone to artifacts and attenuation, and longer scan times, it is a well-established technique compared to PET, and has been extensively used in clinical routine since 1990s. Moreover, SPET installation demands much lower cost and SPET tracers are widely available. On the other hand, the use of PET is still limited as it is associated with very high cost. More importantly there is great difficulty in the distribution of the very short physical half-life of PET tracers used in neuroimaging (e.g. C^{11}, FLT) [7]. Hence, given the advantages and disadvantages of each modality, SPECT will maintain an exclusive standing in clinical diagnosis, as it is a widely used modality with robust outcomes.

The existing imaging techniques (anatomic, metabolic, functional, etc.) provide valuable information for the diagnosis and progression of brain lesions. However, every single one of these imaging methods presents limitations and hence may not be sufficient to give a complete picture of the lesions profile. The combination of both morphologic imaging modalities and functional, metabolic, or molecular imaging techniques may improve the sensitivity, specificity and diagnostic accuracy during the evaluation of brain lesions and consequently optimize the treatment schemes provided to each patient. Hence, a diagnostic preoperative protocol that combines all the above techniques can lead to a more objective and realistic preoperative approach. In this work we sought to investigate the feasibility of such a protocol for the pre-operative evaluation of brain tumors.

Subjects and methods

Subjects

Our prospective clinical study was approved by the hospital institutional review board and informed consent was obtained from all patients studied. Sixty-one patients were included in the study with various intracranial lesions. The patients underwent ^{1}H-MRS, DWI, DTI and DSC MRI followed by ^{99m}Tc-Tetrofosmin brain SPET within the same week. All advanced MR techniques were evaluated by a radiologist and processed by a medical physicist and brain SPET images were evaluated by a nuclear medicine physician and processed by a medical physicist. Nevertheless, it has to be stressed that the advanced MR techniques require a 40-minute to 1hour protocol, including ^{1}H-MRS which demands perfect immobilization of the patient in order to obtain spectra from small volumes of tumor tissue. In addition, *^{99m}Tc-Tetrofosmin brain SPET is also a time consuming process given that the scanning time is approximately 30 minutes for both early and delayed scanning with a total* waiting of three hours. Hence, the demanding requirements of both MRI and brain SPET protocols unfortunately excluded twenty-four patients from the preliminary cohort due to inability of patient immobilization or involuntary movement. Eventually thirty-six adult patients were included in our study, 17 males and 19 females.

Patients underwent total or partial surgical resection of their lesions with the aid of a frameless neuro-navigational system in our institution and the surgical procedures were performed within a month from the neuroimaging analysis. A histopathological diagnosis was obtained in these cases and was compared with our imaging results.

Conventional MR imaging, ^{1}H-MRS, DWI, DTI and DSCE examination protocols

All imaging was performed using the 3-T MR whole-body scanner (Signa HDx; GE Healthcare, Waukesha, WI, USA) applying a standardized MRI, ^{1}H-MRS, DWI, DTI and DSCE examination patient protocol with a 4-channel birdcage and an 8-channel phased-array head coil. Standard anatomic MRI sequences included pre-contrast sagittal, transverse and coronal T2-weighted FSE (repetition time (TR)/echo time (TE) 4800ms/103ms, slice thickness 3mm), pre-contrast axial T2-weighted fluid attenuation inversion recovery (FLAIR) (TR/TE 9502ms/126ms, slice thickness 5mm), pre and post-contrast axial T1-weighted FSE images (TR/TE 700ms/9.4ms, slice thickness 5mm) were also obtained, post-contrast isotropic 3-dimensional spoiled gradient echo (3D-SPGR, TR/TE 6.8ms/2.1ms, 12^{0} flip angle, 240×240mm^{2} field of view (FOV), 136 slices of 1.2mm thickness)

Diffusion MRI

DWI used a single-shot, spin-echo, echo planar sequence (TR/TE 10000/72.6ms, flip angle 90^{0}, FOV 220×220mm, slice thickness 3mm) using b values of 0 and 1000 s/mm^{2}. DTI was performed prior to contrast media injection, in the axial plane with single-shot spin-echo, echo planar sequence (TR/TE 8000ms/99.8ms, flip angle 90^{0}, FOV 220×220mm, slice thickness 3mm with gap=1mm and NEX=1,b=0 and 1000s/mm^{2}) with gradients applied in 25 nonlinear directions.

DSC MRI

DSC perfusion imaging was performed during the first pass of bolus of contrast (5mL/sec) material at a dose of >0.4mmol/kg body weight with a single shot gradient-echo, echo planar imaging sequence (TR/TE 2.000/20.7ms, flip angle=60^{0}, FOV 220×220mm, slice thickness 3mm with gap=0mm, NEX=1). The section thickness and location of the perfusion weighted MR data set were determined by using axial T1-weighted images after contrast injection to locate the lesion.

^{1}H-MR spectroscopy

PRoton Brain Exam (PROBE) Single-Voxel (SV) spectroscopy and two-dimensional-MRSI (2D-MRSI) were performed before contrast administration in order to avoid signal disturbance. Data were acquired using Point-RESolved Spectroscopy (PRESS) pulse sequence with phase-encoding gradients in two directions. Automatic shimming and Gaussian water suppression were used. Measurement parameters used in single-voxel scans were TR/TE 1.500/35ms, 128 signal acquisitions (Nacq). The voxel of interest (VOI) was manually placed on one of the most central slices in the intratumoral area and localized by using the transverse T2-weighted FLAIR or T2-weighted FSE, sagittal and coronal T2-weighted FSE imaging sequences. The location of the VOI was selected to analyze the most homogeneous or representative part of the tumor. The voxel size was adjusted to the size and extent of each lesion and was chosen not to be less than 3.375cm^{3} (i.e. minimum voxel size 1.5x1.5x1.5 cm) for adequate SNR. The contralateral normal area

(cNA) was used as the control spectrum. Measurement parameters used in 2D-CSI were TR/TE 1000/144ms, phase-encoding steps 16×16 and the FOV size was adjusted to the patient's anatomy. Single-voxel PRESS was acquired in all cases while multi-voxel CSI was not always technically successful.

^{99m}Tc-Tetrofosmin brain SPET

Brain SPET images were obtained approximately 20 minutes (early images) and 3 hours (delayed images) after intravenous injection of 25mCi(925MBq) radiotracer activity. The radiopharmaceutical was prepared in the department of Nuclear Medicine of our hospital using Myoview™ powder kit (General Electric, Healthcare Ltd) that was reconstituted with ^{99m}Technetiumpertechnetate ($^{99m}TcO_4^-$) sterile solution. All images were acquired using a dual-head gamma camera (Infinia, General Electric Healthcare) with parallel-hole collimators of high resolution. The photopeak was centered at 140 keV, using a symmetrical 10% window and acquisition time30s per frame. The images were collected in a 128×128 matrix with a Butterworth filtered back-projection algorithm to reduce statistical noise. The algorithm reconstructed raw data in sagittal, transverse and coronal tomographic view.

Data post-processing

DWI, DSC, ^{1}H-MRS

All advanced MRI techniques were performed on the Advantage Linux workstation using the Functool software (General Electric Healthcare).

ADC maps were acquired from isotropic DWI and FA maps were acquired from DTI.ROIs were placed manually in the intratumoral and contralateral region of each lesion using T2-weighted, T2-weighted FLAIR and T1-weighted post-contrast images as reference images to guide the accurate ROI placement. Minimum ADC values and maximum FA values were obtained from ROIs (approximate size 50mm^2) manually placed within each tumor taking care that ROIs were not placed over areas of inhomogeneous susceptibility.

For DSC-MRI, T2*-weighted images were firstly corrected for motion artifacts with BrainStat software. The CBV map (approximated by using the negative enhancement integral) was then overlaid on T2-weighted or T1 post-contrast images. ROIs were placed in the intratumoral region (approximate size 50mm^2) each presenting increased perfusion, as seen on the CBV colored overlay maps. Normal-appearing white matter ROI were placed in the contralateral hemisphere and a maximum CBV ratio was finally calculated (Lesion/Normal ratio).

Post-processing of spectral data was performed on GE workstation with the Functool software. Spectra for each patient were acquired from the intratumoral region. For both SV and 2D-MRSI a cubic VOI and a rectangular ROI respectively were localized by using the transverse T2-weighted FLAIR or T2-weighted FSE, sagittal and coronal T2-weighted FSE imaging sequences. Control VOIs and ROIs were placed in the mirror image location in the contralateral hemisphere. Post-processing of the raw spectral data included baseline correction, frequency inversion and phase shift. Gaussian curves were fitted to NAA, Cho, Cr, lipid and myo-inositol peaks for determination of peak area. Maximum peak-height ratios were recorded for NAA/Cr, Cho/Cr and mI/Cr for each VOI and ROI separately, from single-voxel and 2D MRSI, respectively.

^{99m}Tc-Tetrofosmin brain SPET

Post-processing of brain SPET images was performed on GE workstation with the Xeleris software (General Electric Healthcare). *The early SPET images were co-registered with* T2-weighted FLAIR or *post-contrast T1-weighted images, in cases of low radiotracer uptake, in order to locate the lesion's extent and margins.*

Firstly, a ROI was drawn over the slice with the greatest ^{99m}Tc-Tetrofosmin uptake, in the transverse plane of the reconstructed raw data. The ROI placement within the tumor was carefully performed. For this purpose, combined information from post-contrast T1-weighted images and T2-weighted FSE or brain SPET and MRI fusion *images was used. The ROI was manually defined around the lesion in order to enclose the areas with the highest tracer uptake. An identical control ROI was placed on the contralateral normal parenchyma. Following, three consecutive transverse slices* showing the *highest* tracer *uptake were manually* summed and the same method of ROI delineation was applied.

^{99m}Tc-Tetrofosmin index was defined as the ratio of average counts in the tumor to that in the normal parenchyma in both methods (Lesion/Normal ratio).

Statistical analysis

Quantitative variables were expressed as mean values (SD), while qualitative variables were expressed as absolute and relative frequencies. Student's t-tests and analysis of variance (ANOVA) were computed for the comparison of mean values. Bonferroni correction was used in order to control for type I error. Pearson correlations coefficients were used to explore the association of two continuous variables. ROC curve (Receiver operating characteristic curves) was used in order to estimate the discriminative ability of FA values for high grade tumors. Sensitivity and specificity were calculated for optimal cut-offs. The area under the curve (AUC) was also calculated. All reported p values are two-tailed. Statistical significance was set at $p<0.05$ and analyses were conducted using SPSS statistical software (version 19.0).

Results

Sample consisted of 36 patients (17 men and 19 women) with mean age 52.8 years (SD=14.2). 55.6% of the patients had GBM, 25% meningioma and 13.9% metastatic tumor. In twenty-eight cases (77.8%) the tumor was high grade (Table 1). The differences in SPET and MRI imaging variables between low- and high-grade tumors are presented in Table 2. Only FA values were found to be significantly different between low- and high-grade tumors, with low grade tumors

Table 1. Demographics and clinical characteristics

	N (%)
Sex	
Women	19 (52.8)
Men	17 (47.2)
Age, mean (SD)	52.8 (14.2)
Diagnosis	
GBM	20 (55.6)
Meningioma	9 (25.0)
Metastases	5 (13.9)
Neurocytoma	1 (2.8)
Lymphoma	1 (2.8)
Grade	
High	28 (77.8)
Low	8 (22.2)

having greater values. ROC analysis was performed in order to find the optimal cut-off for FA values in order to discriminate low from high grade tumors. The AUC was 0.92 (95% CI: 0.82-1.00; P<0.001) (Figure 1). The optimal cut-off value for FA was 0.11 with sensitivity 100.0% and specificity 82.1%.

Ml/Cr values were significantly positively correlated with NAA/Cr and Cho/Cr values (Table 3). Thus higher ml/Cr values are associated with higher NAA/Cr and Cho/Cr values. Also, higher ADC values are significantly associated with lower NAA/Cr and FA values. Higher rCBV values were significantly associated with higher early and delayed SPET values (Figures 2 and 3). In addition, higher early SPET values were significantly associated with higher delayed SPET values.

The differences in SPET and MRI imaging variables according to diagnosis are presented in Table 4. There were significant differences in NAA/Cr, FA and ADC values among the diagnoses. More specifically, after Bonferroni correction, it was found that patients with GBM had significantly lower NAA/Cr values compared to those with meningioma and those with metastases. Moreover, patients with meningioma had significantly higher FA values compared to those with GBM and those with metastases. On the contrary, patients with meningioma had significantly lower ADC values compared to those with GBM and those with metastases.

Table 2. Differences in SPET and MRI imaging variables between low- and high-grade tumors

	Grade		P⁺
	High	Low	
	Mean (SD)	Mean (SD)	
MRS			
NAA/Cr	1.11 (0.19)	1.21 (0.32)	0.312
Cho/Cr	1.55 (0.50)	1.53 (0.57)	0.918
mI/Cr	1.00 (0.15)	1.00 (0.22)	0.967
DWI			
FA	0.08 (0.03)	0.18 (0.09)	**<0.001**
ADC (e-09)	1.60 (0.58)	1.23 (0.40)	0.101
DSC			
rCBV	4.36 (2.06)	4.86 (2.86)	0.565
SPECT			
EARLY(L/N)	5.47 (3.01)	5.23 (3.95)	0.852
LATE (L/N)	5.98 (3.37)	5.16 (4.42)	0.574

⁺*Student's t-test*

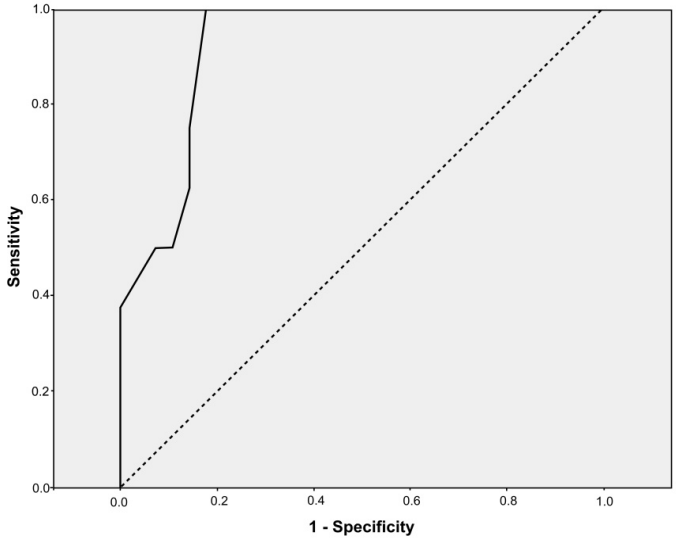

Figure 1. ROC curve for the discrimination of high-grade tumors from FA values

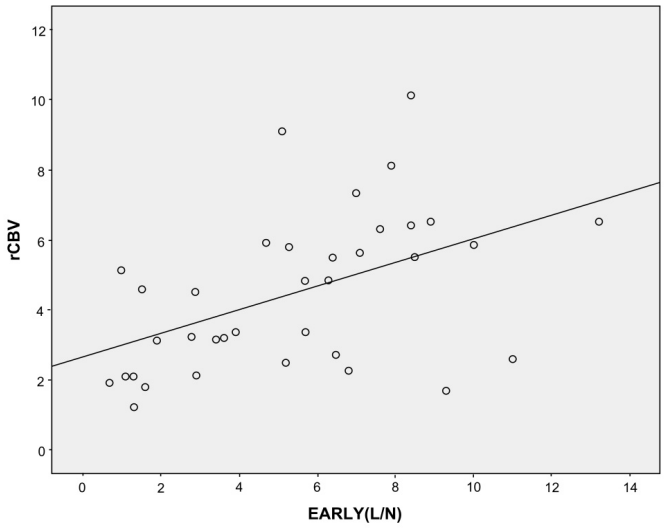

Figure 2. Correlation between rCBV values and early SPET values

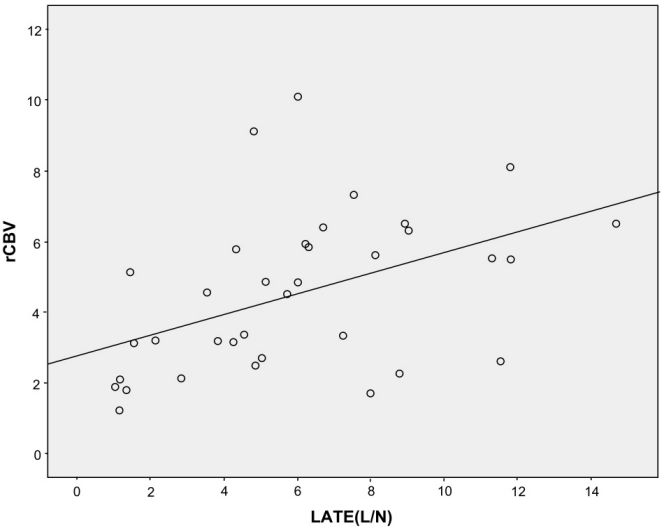

Figure 3. Correlation between rCBV values and late SPET values

Paired comparison among early and delayed SPET index showed that delayed SPECT L/N ratios were significantly increased in GBM tumors (P=0.018). On the contrary, delayed SPET values were not significantly different in comparison with early SPET values in meningiomas (P=0.125) and metastatic tumors (P=0.247).

Discussion

In our study, a significant positive correlation was observed between rCBV and ^{99m}Tc-Tetrofosmin uptake in both early and delayed images, which is in agreement with previously reported findings [8,9,10]. ^{99m}Tc-Tetrofosmin uptake depends on regional blood flow and blood-brain barrier (BBB) permeability. Relative cerebral blood volume (rCBV) obtained by dynamic susceptibility contrast (DSC)-MRI is also based on tumor perfusion and angiogenesis [11]. Thus, both ^{99m}Tc-Tetrofosmin uptake and rCBV may quantify vascular proliferation which is related to tumor malignancy according to previous reports [12,13]. Tomoi et al. used DSC MRI and ^{99m}Tc-HSA-D SPET to assess

Table 3. Correlation between the SPET and MRI imaging variables

	MRS			DWI		DSC	SPET	
	NAA/Cr	**Cho/Cr**	**mI/Cr**	**FA**	**ADC (e-09)**	**rCBV**	**EARLY(L/N)**	**LATE (L/N)**
MRS								
NAA/Cr	1.00	-0.10	0.48**	0.28	-0.38*	0.19	0.37*	0.08
Cho/Cr		1.00	0.33*	-0.01	0.05	0.13	-0.04	0.08
mI/Cr			1.00	0.11	-0.28	0.16	0.02	-0.06
DWI								
FA				1.00	-0.40*	-0.05	-0.04	-0.17
ADC (e-09)					1.00	-0.24	-0.23	-0.14
DSC								
rCBV						1.00	0.48**	0.47**
SPET								
EARLY(L/N)							1.00	0.88***
LATE (L/N)								1.00

P<.05;P<.01;***P<.001*

Table 4. Differences in SPET and MRI imaging variables according to diagnosis

	Diagnosis			P^{+}	P^{++} GBM vs. Meningioma	P^{++} GBM vs. Metastases	P^{++} Meningioma vs. Metastases
	GBM	**Meningioma**	**Metastases**				
	Mean (SD)	Mean (SD)	Mean (SD)				
MRS							
NAA/Cr	1.05 (0.17)	1.29 (0.16)	1.31 (0.20)	0.002	0.005	0.021	>0.999
Cho/Cr	1.70 (0.50)	1.51 (0.54)	1.28 (0.23)	0.206	>0.999	0.274	>0.999
mI/Cr	1.01 (0.14)	1.03 (0.21)	1.03 (0.15)	0.907	>0.999	>0.999	>0.999
DWI							
FA	0.08 (0.03)	0.17 (0.09)	0.07 (0.02)	<0.001	<0.001	>0.999	0.005
ADC (e-09)	1.59 (0.55)	1.03 (0.25)	1.96 (0.54)	0.004	0.024	0.428	0.006
DSC							
rCBV	4.33 (1.68)	5.89 (2.99)	3.48 (1.78)	0.093	0.221	>0.999	0.145
SPET							
EARLY(L/N)	5.23 (2.97)	7.14 (3.30)	4.50 (3.14)	0.219	0.393	>0.999	0.402
LATE (L/N)	6.32 (3.58)	6.47 (3.70)	4.10 (3.10)	0.429	>0.999	0.665	0.726

$^{+}$ANOVA $^{++}$pairwise comparisons after Bonferroni correction

the radio-therapeutic effect on brain tumors; their research showed that the indices describing tumor vascularity of the brain correlated well between DSC MRI and ^{99m}Tc-HSA-D SPET while DSC MRI provides information on radiation effects that is not available with conventional MRI [14]. Examining a larger patient population, in a more recent study, Alexiou et al. investigated the use of ^{99m}Tc-Tetrofosmin, DTI and DSCI for glioma grading [8]. They reported a strong correlation of rCBV and ADC to ^{99m}Tc-Tetrofosmin uptake as well as a significant correlation of all parameters to cellular proliferation. All techniques significantly differentiated low-grade from high-grade gliomas, however the authors highlighted that DSC MRI and ^{99m}Tc-Tetrofosmin metrics were more indicative of glioma grade [8]. In a similar study, using the same modalities for the detection of recurrent high-grade gliomas, Alexiou and colleagues reported a strong positive correlation between ^{99m}Tc-Tetrofosmin uptake and rCBV, while DTI was found to be inferior to DSC MRI and brain SPET [10].

Moreover, in our study, delayed SPET L/N ratios were significantly increased compared to early SPECT L/N ratios in glioblastomas multiforme, whilst ^{99m}Tc-Tetrofosmin index from delayed and early images was not significantly different in meningiomas and metastatic tumors. Sun and colleagues examined a vast cohort of patients using ^{201}Tl brain SPET. Healthy subjects showed little scattered radioactivity in the brain parenchyma while brain hematomas presented high tracer uptake on early images but radioactivity decreased remarkably on delayed scans. Benign lesions and low grade tumors presented stable or slightly decreasing tracer uptake while radioactivity increased in high grade and metastatic tumors on delayed images [15]. These findings agree with our results, except for metastatic tumors, and may suggest that the early tracer uptake depends on perfusion and BBB permeability of the lesion but the tracer retention on delayed images may involve additional mechanisms; tumor cell membrane adenosine triphosphatase pump and mitochondrial content may play a significant role on tracer retention [16,17].^{201}Thallium and ^{99m}Tc-labelled compounds have similarities in terms of uptake mechanism; they passively accumulate in cells characterized by higher metabolic activity. Given that tumor cells present higher mitochondrial density and higher transmembrane electrical potential than the surrounding tissue these radiopharmaceuticals accumulate more intensely in malignant tumors [18,19]. Furthermore, Jinnouchi et al. concluded that high ^{201}Tl retention may predict malignant potential in meningiomas, while Kinuya and colleagues reported that delayed L/N ratio of glioblastoma multiforme was significantly high comparing to brain abscesses [20,21]. Consequently, delayed tracer uptake may be indicative for tumor malignancy and not simply for BBB breakdown.

^{99m}Tc-labelled compounds have been used as an alternative to ^{201}Thallium to evaluate brain tumor metabolism [22,23]. ^{99m}Tc-labelled compounds are lipophilic cationic complexes and they have proved to be efficient tumor-seeking agents. Shibata and colleagues compared the diagnostic value of ^{201}Thallium and ^{99m}Tc-MIBI SPET in glioma diagnosis. The authors suggested that ^{99m}Tc-MIBI SPET with delayed

acquisition is the most cost-effective choice as this method yielded more favorable results; however, both SPET modalities may produce false positive and negative findings in glioma diagnosis [19].

In our study, both early and delayed ^{99m}Tc-Tetrofosmin L/N ratios were higher in high-grade lesions (5.47 and 5.97, respectively) compared to low-grade tumors (5.23 and 5.16, respectively) but they could not solely determine the differential diagnosis. The main drawback in lesions differentiation with SPET modalities is the heterogeneous form of malignant tumors, especially glioblastomas, and the presence of internal necrosis leading to false negative tracer uptake. Moreover, some benign intracranial tumors show high activity of sodium potassium (Na^+/K^+) adenosine triphosphatase on cell membranes through unknown mechanisms, leading to high tracer uptake [24]. In addition, ^{99m}Tc-labeled compounds are physiologically undertaken by orbita, nasopharyngeal tissues, pituitary, scalp and choroid plexus and therefore the detection and delineation of small lesions especially in the deep para-ventricular space may be challenging [25].

Regarding ^{1}HMRS, there were significant differences in NAA/Cr among lesions. NAA is recognized as a marker of functional neurons and their appendages and its reduction is caused by any destructive, degenerative or infiltrative process [12]. Cho on the other hand, increases by pathological changes in membrane turnover or rapid cell division [26]. GBMs are characterized by markedly reduced NAA and an increase in the Cho peak [27]. In our study, GBMs showed an increase in the Cho/Cr ratio and NAA/Cr was significantly lower in GBMs compared to meningiomas and metastatic tumors. On the other hand, both early and delayed Tetrofosmin uptake was lower in GBMs (Early L/N=5.23 and Delayed L/N=6.32) and metastatic tumors (Early L/N=4.50 and Delayed L/N=4.10) compared to meningiomas (Early L/N=7.14 and Delayed L/N=6.47). However, GBMs and metastases with low tracer uptake showed a distinct peak of lipids in the ^{1}H-MR spectrum which proves that internal necrosis may lead to false negative results in brain SPET. Indicatively Figure 4 depicts a 56 years old woman with GBM; the rCBV map and the ^{99m}Tc-Tetrofosmin brain SPET and MRI fusion image show high gadolinium uptake and high tracer uptake respectively in the tumor periphery and minimum uptake in the center of the tumor, while ^{1}H-MR spectrum shows a distinct lipid peak inside the tumor. Therefore, a ROI that delineates the whole tumor volume in ^{99m}Tc-Tetrofosmin SPET may not always be representative of the tumor malignancy due to heterogeneities, especially in GBMs.

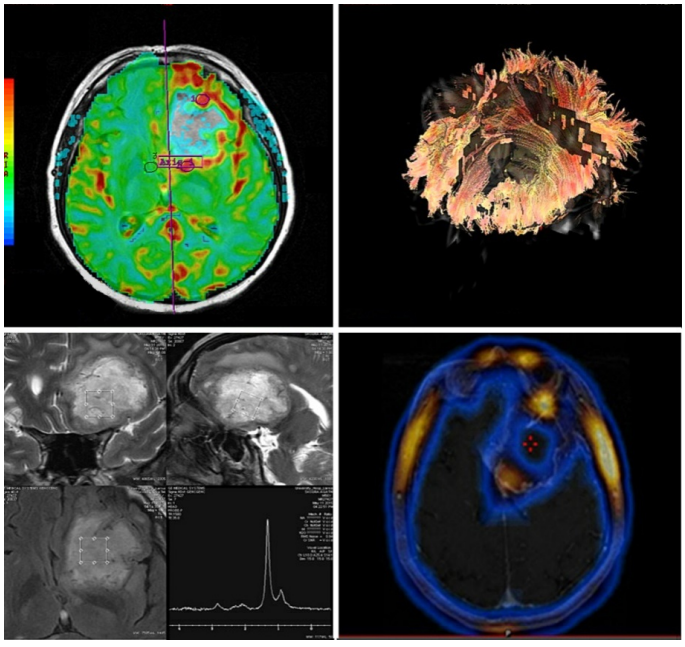

Figure 4. A 56 years old woman with GBM A) rCBV map shows high gadolinium uptake in the tumor periphery and minimum uptake in the center of the tumor B) fiber tractography shows fiber displacement and disruption inside the tumor C) single VOI pictured in transverse, sagittal and coronal plane, short echo time spectrum shows high lipid peak D) ^{99m}Tc-Tetrofosmin brain SPET and MRI fusion image shows high tracer uptake in the tumor periphery and minimum tracer uptake in the center of the tumor

Patients with meningioma had significantly higher FA values and respectively significantly lower ADC values compared to those with GBM and those with metastases. Moreover, FA values were found to be significantly different between low and high grade tumors and the optimal cut-off value for FA, after ROC analysis, was 0.11. The high-grade tumors sample consisted of GBM, metastatic tumors and atypical meningiomas, while the low grade tumors cohort included typical meningiomas, one lymphoma and one neurocytoma. Fractional anisotropy describes the degree of water directionality inside a voxel [28]. Previous studies have shown that ADC and FA may be considered as indices of cell density, contributing in noninvasive tumor grading [29]. High grade tumors show tumor heterogeneities with necrotic and cystic regions which result in reduction of the directionality of water diffusion, a process reflected as a decrease in FA values [12]. However, conflicting results are found in employing FA to predict tumor malignancy or lesion differentiation. Inoue et al. and Lee et al. studied the use of FA values in glioma grading and reported a trend towards higher FA values in HGG relative to LGG [30,31]. On the other hand, FA values are affected by several factors such as the density and composition of tumor cells, vascularity and fiber structure resulting in inability to discriminate lesions.

Our study had several limitations; the cohort of patients was limited due to the demanding requirements of both MRI and brain SPET protocols especially in terms of immobilization and cooperation. Moreover, our sample of low-grade lesions consisted of only 8 cases and therefore we could not conduct a robust outcome in relation to high-grade tumors (28 cases). However, to the best of our knowledge this is the first report describing the relationship between all the advanced MRI techniques with both early and delayed *^{99m}Tc-Tetrofosmin* brain SPET

Conclusion

Only delayed ^{99m}Tc-Tetrofosmin brain SPET compared to early ^{99m}Tc-Tetrofosmin brain SPET images especially when combined with advanced MR techniques showed promise in the differential diagnosis between high- and low-grade tumors.

References

1. Kousi E, Tsougos I, Kapsalaki E (2013) Proton Magnetic Resonance Spectroscopy of the Central Nervous System. In: Fountas K, ed. Novel Frontiers of Advanced Neuroimaging. InTech; 2013: 19-50.

2. Heiss WD, Raab P, Lanfermann H (2011) Multimodality assessment of brain tumors and tumor recurrence. *J Nucl Med* 52: 1585-1600. [Crossref]

3. Al-Okaili RN, Krejza J, WangS et al. (2006) Advanced MR Imaging Techniques in the Diagnosis of Intraaxial Brain Tumors in Adults. *RadioGraphics* 26: 173-89.

4. Farjam R, Tsien CI, Feng FY, Gomez-Hassan D, Hayman JA, et al. (2014) Investigation of the diffusion abnormality index as a new imaging biomarker for early assessment of brain tumor response to radiation therapy. *Neuro Oncol* 16: 131-139. [Crossref]

5. Tsolaki E, Kousi E, Svolos P et al. (2014) Clinical decision support systems for brain tumor characterization using advanced magnetic resonance imaging techniques.*World J Radiol* 6:72-81.

6. Soares JM, Marques P, Alves V, Sousa N. (2013) A hitchhiker's guide to diffusion tensor imaging. *Front Neurosci* 7:31.

7. Rahmim A, Zaidi H (2008) PET versus SPECT: strengths, limitations and challenges. *Nucl Med Commun* 29: 193-207. [Crossref]

8. Alexiou GA, Zikou A, Tsiouris S, Goussia A, Kosta P, et al. (2014) Correlation of diffusion tensor, dynamic susceptibility contrast MRI and (99m)Tc-Tetrofosmin brain SPECT with tumour grade and Ki-67 immunohistochemistry in glioma. *Clin Neurol Neurosurg* 116: 41-45. [Crossref]

9. Ernst T, Chang L, Itti L, Speck O (1999) Correlation of regional cerebral blood flow from perfusion MRI and spect in normal subjects. *Magn Reson Imaging* 17: 349-354. [Crossref]

10. Alexiou GA, Xourgia X, Vartholomatos E, Tsiouris S, Kalef-Ezra JA, et al. (2014) Comparison of (99m)tc-tetrofosmin and (99m)tc-sestamibi uptake in glioma cell lines: the role of p-glycoprotein expression. *Int J Mol Imaging* 2014: 471032. [Crossref]

11. Schellinger PD, Warach S. (2005) Seeing the Brain So We Can Save It: The Evolution of Magnetic Resorance Imaging as a Clinical Tool. In: Waxman S, ed.From Neuroscience To Neurology: Neuroscience, Molecular Medicine, and the Therapeutic Transformation of Neurology.Burlington; Academic Press, 2005:3-19.

12. Tsougos I, Svolos P, Kousi E et al. (2012) Differentiation of glioblastoma multiforme from metastatic brain tumor using proton magnetic resonance spectroscopy, diffusion and perfusion metrics at 3 T. Cancer Imaging 26:423-36.

13. Lorger M (2012) Tumor microenvironment in the brain. *Cancers (Basel)* 4: 218-243. [Crossref]

14. Tomoi M, Maeda M, Yoshida M, Yamada H, Kawamura Y, et al. (1999) Assessment of radiotherapeutic effect on brain tumors by dynamic susceptibility contrast MR imaging: a preliminary report. *Radiat Med* 17: 195-199. [Crossref]

15. Sun D, Liu Q, Liu W, Hu W (2000) Clinical application of 201Tl SPECT imaging of brain tumors. *J Nucl Med* 41: 5-10. [Crossref]

16. Sato T, Indo H, Kawabata Y, Kobayashi T, Suenaga S, et al. (2005) Thallium-201 chloride (Tl-201) accumulation and Na+/K+-ATPase expression in tumours of the head and neck. *Dentomaxillofac Radiol* 34: 212-217. [Crossref]

17. Choi JY, Kim SE, Shin HJ, Kim BT, Kim JH (2000) Brain tumor imaging with 99mTc-tetrofosmin: comparison with 201Tl, 99mTc-MIBI, and 18F-fluorodeoxyglucose. *J Neurooncol* 46: 63-70. [Crossref]

18. Fukumoto M (2004) Single-photon agents for tumor imaging: 201Tl, 99mTc-MIBI, and 99mTc-tetrofosmin. *Ann Nucl Med* 18: 79-95. [Crossref]

19. Shibata Y, Yamamoto T, Takano S, Katayama W, Takeda T, et al. (2009) Direct comparison of thallium-201 and technetium-99m MIBI SPECT of a glioma by receiver operating characteristic analysis. *J Clin Neurosci* 16: 264-269. [Crossref]

20. Jinnouchi S, Hoshi H, Ohnishi T, Futami S, Nagamachi S, et al. (1993) Thallium-201 SPECT for predicting histological types of meningiomas. *J Nucl Med* 34: 2091-2094. [Crossref]

21. Kinuya K, Ohashi M, Itoh S, Yamamoto K, Sakai S, et al. (2002) Differential diagnosis in patients with ring-like thallium-201 uptake in brain SPECT. *Ann Nucl Med* 16: 417-421. [Crossref]

22. Maffioli L, Steens J, Pauwels E, Bombardieri E (1996) Applications of 99mTc-sestamibi in oncology. *Tumori* 82: 12-21. [Crossref]

23. Tsiouris S, Alexiou G, Papadopoulos A, Fotopoulos A. (2011) Metabolic Imaging of Brain Tumor by 99mTc-Tetrofosmin Scintitomography. In: Abujamra AL, ed. Diagnostic Techniques and Surgical Management of Brain Tumors. InTech; 2011:303-24.

24. Kanamori M, Kumabe T, Shimizu H, Yoshimoto T (2002) (201)Tl-SPECT, (1)H-MRS, and MIB-1 labeling index of central neurocytomas: three case reports. *Acta Neurochir (Wien)* 144: 157-163. [Crossref]

25. Filippi L, Santoni R, Manni C et al. (2005) Imaging Primary Brain Tumors by Single-Photon Emission Computerized Tomography (SPECT) with Technetium-99m Sestamibi (MIBI) and Tetrofosmin. *Curr Med Imaging Rev* 1: 61-6.

26. Soares DP, Law M (2009) Magnetic resonance spectroscopy of the brain: review of metabolites and clinical applications. *Clin Radiol* 64: 12-21. [Crossref]

27. Lobanov IA, Shakhov BE, Medyanik IA, Fraerman AP. (2013) Proton magnetic resonance spectroscopy in differential diagnosis of brain tumors. ?linical Medicine 5: 72-6.

28. Tsitsia V, Svolou P, Kapsalaki E, Theodorou K, Vassiou K, et al. (2017) Multimodality-multiparametric brain tumors evaluation. *Hell J Nucl Med* 20: 57-61. [Crossref]

29. Reiche W, Schuchardt V, Hagen T, Il'yasov KA, Billmann P, et al. (2010) Differential diagnosis of intracranial ring enhancing cystic mass lesions--role of diffusion-weighted imaging (DWI) and diffusion-tensor imaging (DTI). *Clin Neurol Neurosurg* 112: 218-225. [Crossref]

30. Inoue T, Ogasawara K, Beppu T, Ogawa A, Kabasawa H (2005) Diffusion tensor imaging for preoperative evaluation of tumor grade in gliomas. *Clin Neurol Neurosurg* 107: 174-180. [Crossref]

31. Lee EJ, Lee SK, Agid R, Bae JM, Keller A, et al. (2008) Preoperative grading of presumptive low-grade astrocytomas on MR imaging: diagnostic value of minimum apparent diffusion coefficient. *AJNR Am J Neuroradiol* 29: 1872-1877. [Crossref]